Nanoscale Horizons

ROYAL SOCIETY OF CHEMISTRY

COMMUNICATION

View Article Online
View Journal | View Issue

Check for updates

Cite this: *Nanoscale Horiz.*, 2026, **11**, 539

Received 14th July 2025,
Accepted 23rd October 2025

DOI: 10.1039/d5nh00489f

rsc.li/nanoscale-horizons

Published on 28 Oktober 2025. Downloaded on 24.02.26 18:29:01.

Noncovalent and precise loading of small molecule drugs on DNA nanocarriers

Xinyu Feng,[a] Mingtao Zhao,[d] Huichao Chen,[a] Rui She,[a] Yangying Wang,[a] Leyi Jia,[a] Wenting Li,[a] Mengmeng Li,[a] Shuheng Wei,[d] Yunxiao Ma,[a] Wuyi Sun,*[a] Xiao Cui,*[b] Song Wang*[c] and Jiemin Zhao *[ab]

DNA nanocarriers have been utilized for delivering a variety of functional cargo molecules, demonstrating unique properties such as designable and programmable structures, site-specific functionality, and superior biocompatibility. However, nucleic acid nanocarriers present significant limitations when it comes to loading small molecule drugs. Covalent integration of small molecule drugs into nucleic acid nanocarriers usually requires complex organic chemical reactions. Here we report a new method that enables the noncovalent and precise loading of small molecule drugs onto DNA nanocarriers. This is achieved through the formation of small molecule-mediated non-canonical base pairing. As a proof of principle, we successfully loaded cordycepin into aptamer-functionalized DNA nanoparticles and achieved a significant therapeutic effect in melanoma-bearing mice. This approach expands the range of small molecule drugs that can be loaded onto DNA nanostructures, particularly benefiting the synergistic therapy that combines small molecule drugs with nucleic acid drugs.

New concepts

In this study, we report an innovative noncovalent conjugation strategy to precisely load small molecule drugs in DNA nanocarriers. This is accomplished by integrating the small molecule drugs into the DNA structures through the formation of small molecule-mediated noncanonical base pairs. The common covalent incorporation of small molecule drugs into nucleic acid nanocarriers typically necessitates intricate organic chemical reactions, which may negatively affect the activity, release, and potency of the drugs *in vivo*. We show that the noncovalent conjugation strategy can significantly increase the drug variety available and optimize the drug loading process. Taking cordycepin as an example, the novel DNA nanocarrier generated by rolling circle amplification enables structurally precise and noncovalent drug incorporation. By incorporating an MDR1-specific aptamer, the engineered system demonstrates remarkable tumor suppression in melanoma-bearing mice. This innovation resolves historical loading challenges and preserves drug potency, enabling expanded therapeutic applications of nucleic acid nanocarriers through simplified yet biologically harmonious drug incorporation mechanisms.

1. Introduction

The synergistic therapy strategy of small molecule drugs and functional nucleic acid is receiving significant focus currently.[1] Combinatorial chemo and gene therapy utilizing siRNA or antisense oligonucleotides (ASO) can circumvent drug resistance through suppressing the expression of related proteins, thereby restoring the chemosensitivity of cancer cells.[2,3] The range of this synergistic therapy is broadening beyond cancer treatment to encompass other chronic diseases, such as hypertension and macular degeneration.[4–6] In parallel, nucleic acid aptamers, a distinct type of functional nucleic acid with specific targeting capabilities, have been widely utilized in the design of targeted delivery carriers,[7–10] which can address the deficiencies of small molecule drugs including lack of specificity, limited targeting, poor bioavailability, and pronounced side effects.

The effectiveness of a drug synergistic strategy is highly dependent on the design of nano-vehicles which are capable of simultaneously loading nucleic acid drugs and small molecule drugs with appropriate and controllable loading ratios. Given that nucleic acid drugs can self-assemble into nano-architectures, achieving their carrier-free and precise delivery,[11,12] this approach presents distinct advantages when employed to construct carriers for nucleic acid drugs. However, nucleic acid nanocarriers exhibit significant constraints in the loading of small molecule drugs. Only a very limited selection of small molecule drugs, characterized by a polycyclic aromatic structure, can be integrated into nucleic acid nanocarriers *via*

[a] *School of Pharmacy, Key Laboratory of Anti-inflammatory and Immune Medicine, Ministry of Education, Institute of Clinical Pharmacology, Anhui Medical University, Hefei 230032, China. E-mail: sunwuyi51@aliyun.com, zhaojiemin@ahmu.edu.cn*

[b] *Department of General Surgery, The Second Hospital of Anhui Medical University, Hefei 230601, China. E-mail: cx_2077@vip.sina.com*

[c] *State Key Laboratory of Precision and Intelligent Chemistry, University of Science and Technology of China, Hefei 230026, China. E-mail: wsong09@ustc.edu.cn*

[d] *Second Clinical Medical College, Anhui Medical University, Hefei 230032, China*

Published on 28 Oktober 2025. Downloaded on 24.02.26 18:29:01.

intercalation. For instance, Doxorubicin is routinely employed to illustrate the concept in the development of nucleic acid nanocarriers.[13–15] On the other hand, there are a series of works that utilize organic chemical reactions for covalently attaching small molecule drugs to the nucleic acid backbones or substituting bases when these drugs are nucleoside analogues.[16–19] While these methods have broadened the drug scope that can be loaded onto nucleic acid-based nanocarriers, they necessitate intricate organic reactions. There are also concerns regarding the potential negative impact of covalent linkages on the drug's activity, release and potency *in vivo*. It is important to develop new strategies for small molecule drugs' loading on nucleic acid-based carriers, further expanding drug scope and optimizing the method of drug loading. Recently, we reported a series of small molecule-mediated DNA non-canonical base pairs[20,21] and proposed a high-throughput screening method for these structures, assisted by molecular dynamics simulations. Small molecule-mediated non-canonical base pairing can be incorporated into nucleic acid nanostructures.[20,22] Inspired by this, we proposed a new method that allows for the non-covalent and precise loading of small molecule drugs onto nucleic acid carriers, where the drug molecules are integrated onto the carriers by forming stable triplet structures with bases.

As a proof of concept, we chose cordycepin, a small molecule drug found to mediate T–T base pairing,[21] for incorporation into DNA nanostructures. A compact DNA nanoparticle synthesized through rolling circle amplification[23–28] (RCA) and functionalized with a nucleic acid aptamer was selected to deliver cordycepin for the treatment of melanoma. We demonstrated that our nanocarrier can efficiently load cordycepin and greatly inhibit tumor growth. This work demonstrates a new method for the delivery of small molecule drugs utilizing DNA nano-vehicles, providing a promising delivery strategy for synergistic therapy that integrates nucleic acid drugs and small molecule drugs.

2. Results and discussion

2.1 Cordycepin-mediated T–T base pairing

We initially verified the ability of poly(T) strands to form stable structures with cordycepin. The molecular dynamics (MD) simulations were carried out through our established workflow to investigate the theoretical stability of poly(T)–cordycepin structure.[21] The cordycepin-mediated T6 duplex model (cordycepin-6wk7) and cordycepin replaced DNA triplex model (cordycepin-1bwg) were used as initial simulation models. As illustrated in Fig. 1a, cordycepin can interact with two T residues *via* four hydrogen bonds, two with each T. The geometry and hydrogen bond lengths within each T–cordycepin–T triplet are similar to those of a stable T–A–T triplet (Fig. 1b and Fig. S1–S4). Subsequent experiments further supported these MD simulation results. In native polyacrylamide gel electrophoresis (PAGE), the migration of T_{20} was slower in the presence of cordycepin compared to that in native PAGE without cordycepin (Fig. 1c and d). In the presence of 300 μM cordycepin, the melting temperature (T_m) was 39.7 °C for T_{30}–cordycepin (Fig. 1e and Fig. S5). This observation suggests that T_{20} forms multistranded complexes with cordycepin.

2.2 Synthesis and characterization of RCA-CCS

The DNA nanocarrier loaded cordycepin (CCS) was synthesized through RCA. The linear single-stranded DNA template encoding complementary sequences of an aptamer and a poly(A) region was designed first (Fig. 2). In this study, aptamer d_3[29] was chosen to functionalize our nanocarrier. Aptamer d_3 targets multidrug resistance protein 1 (MDR1), a protein that is overexpressed on the surface of a broad range of cancer cells, causing chemotherapy failure by interfering with drug uptake.[30,31] We incorporated a poly(A) sequence of length 30 into the template to generate a T_{30} region within each replicated unit, providing potential loading sites for cordycepin. Through hybridization with a primer, the linear single-stranded DNA was converted into a circular structure, and the nick was chemically closed *via* T_4 DNA ligation. Native PAGE was used to verify the combination of the template and the primer (Fig. S6). This circular DNA template was subsequently used in rolling DNA amplification. For the synthesis of drug-loaded nanoparticles, cordycepin was added into the reaction system.

The RCA-generated DNA strands then spontaneously folded and condensed, forming nanoparticles. During this process, cordycepin molecules were incorporated into the T-rich regions of the RCA nanoparticles through the formation of T–cordycepin–T triplets. Gel electrophoresis characterization indicated the successful generation of long DNA strands (Fig. 3a). The morphology of the DNA nanoparticles was evaluated using scanning electron microscopy (SEM). As shown in Fig. 3b, in the absence of cordycepin, the elongated single-stranded DNA (ssDNA) spontaneously self-assembled into a cluster structure with an average size of 100 nm. This structure was characterized by several intertwined small particles. We speculated that the unpaired T_{30} sequence in each repeating unit hindered the self-assembly and folding of the elongated ssDNA, resulting in the cluster-like configuration rather than individual spherical particles. Upon the addition of cordycepin, the formation of cordycepin-mediated T–T base pairing within the T_{30} region facilitated the folding of the RCA-generated ssDNA. This led to a morphological change from the cluster-like structure to spherical nanoparticles with an average size of 40 nm. To ensure the reliability of our findings, we evaluated the batch-to-batch reproducibility of the RCA-CCS nanoparticles. We independently synthesized three batches of the material and characterized their morphology and size. As shown in Fig. S7, the RCA-CCS from three different batches all exhibited highly consistent and uniform structures. The data demonstrate our synthesis method in producing nanoparticles with highly reproducible morphology and size. The quantitative analysis of cordycepin incorporation in the nanocarrier was conducted using high performance liquid chromatography (HPLC). The RCA product with cordycepin loading (denoted as RCA-CCS) was extensively washed using an ultrafiltration tube to remove dNTPs and unattached cordycepin. To quantify the contents, the DNA concentration was measured prior to the

 This journal is © The Royal Society of Chemistry 2026

Published on 28 Oktober 2025. Downloaded on 24.02.26 18:29:01.

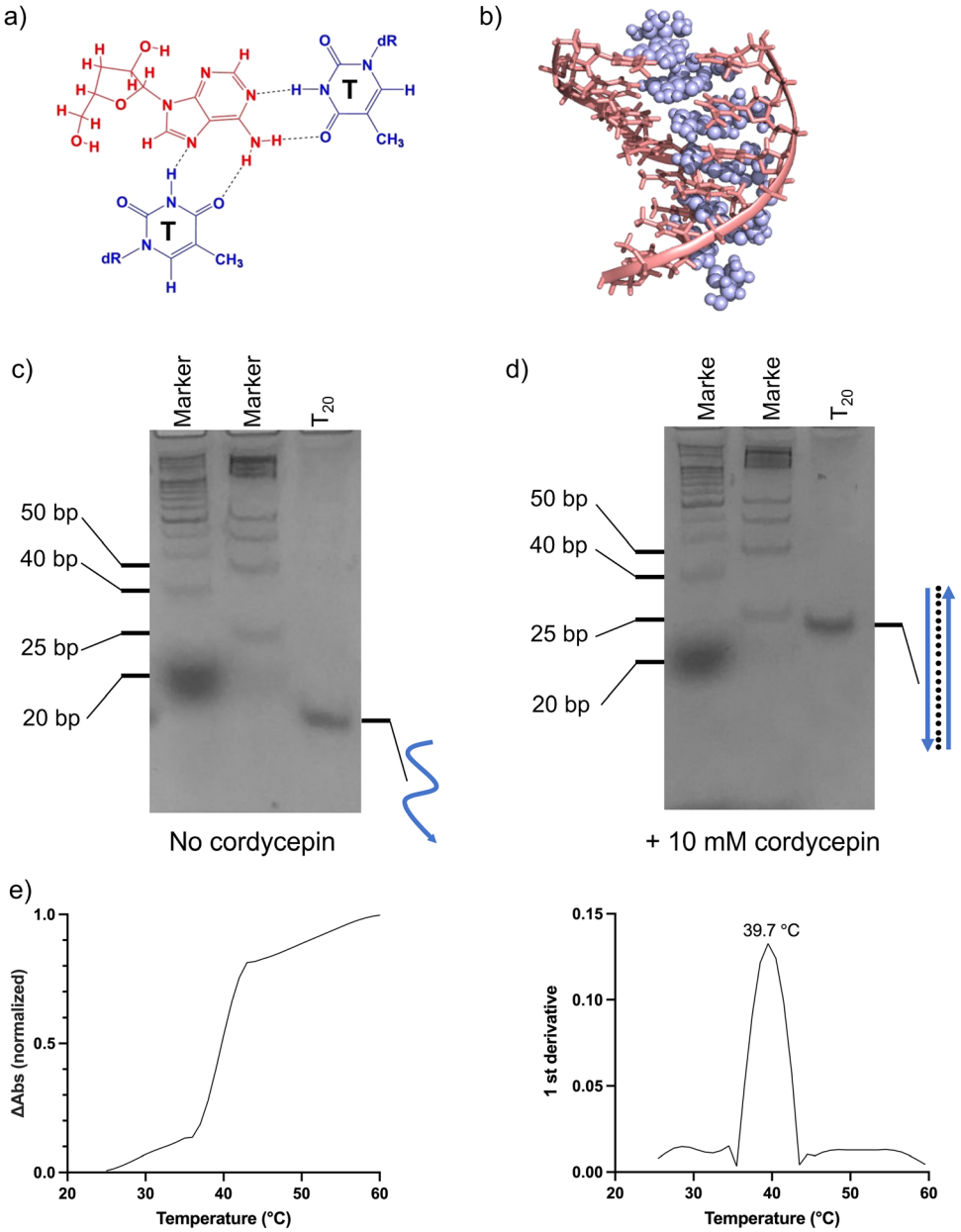

Fig. 1 (a) Structural scheme of T–cordycepin–T triplet; (b) a snapshot of the output from MD simulation of cordycepin-6wk7; (c) and (d) analysis of the cordycepin–T_{20} interaction by native PAGE; (c) without cordycepin in samples and in gel; (d) 10 mM cordycepin in samples and in gel. Sample compositions and the band identities are indicated above and beside the gel images, respectively; (e) UV melting profiles of T–cordycepin–T triplet at 260 nm in 1 × TAE/Mg^{2+} buffer, the concentration of the thymine nucleotide was kept at 60 μM.

DNase treatment of the sample. The quantity of cordycepin present was determined by its peak area (Fig. 3c and Fig. S8). The ratio of cordycepin molecules to the repeating units of RCA product in the sample was found to be 13.3, marginally less than the anticipated theoretical value of 15. This discrepancy was postulated to arise from two reasons: (i) the folding of RCA-generated ssDNA does not ensure that every T base within the T_{30} regions can form cordycepin-mediated T–T base pairing. Therefore, it may not achieve the theoretical value of 15 (half of 30) T–cordycepin–T triplets per RCA repeating unit. (ii) The extensive washing process led to the elution of some cordycepin molecules. The serum stability of RCA nanoparticle was further assessed by gel electrophoresis. The results demonstrated that RCA nanoparticles maintained good stability after being incubated in 10% fetal bovine serum (FBS) for a period of 24 hours (Fig. S9).

2.3 *In vivo* and *in vitro* anti-tumor effect of RCA-CCS

After characterizations, the biocompatibility of the RCA-generated products was evaluated. B16F10 cells were treated with different concentrations of RCA materials for 24 hours. The cell viability remained predominantly unaffected, suggesting the excellent

Published on 28 Oktober 2025. Downloaded on 24.02.26 18:29:01.

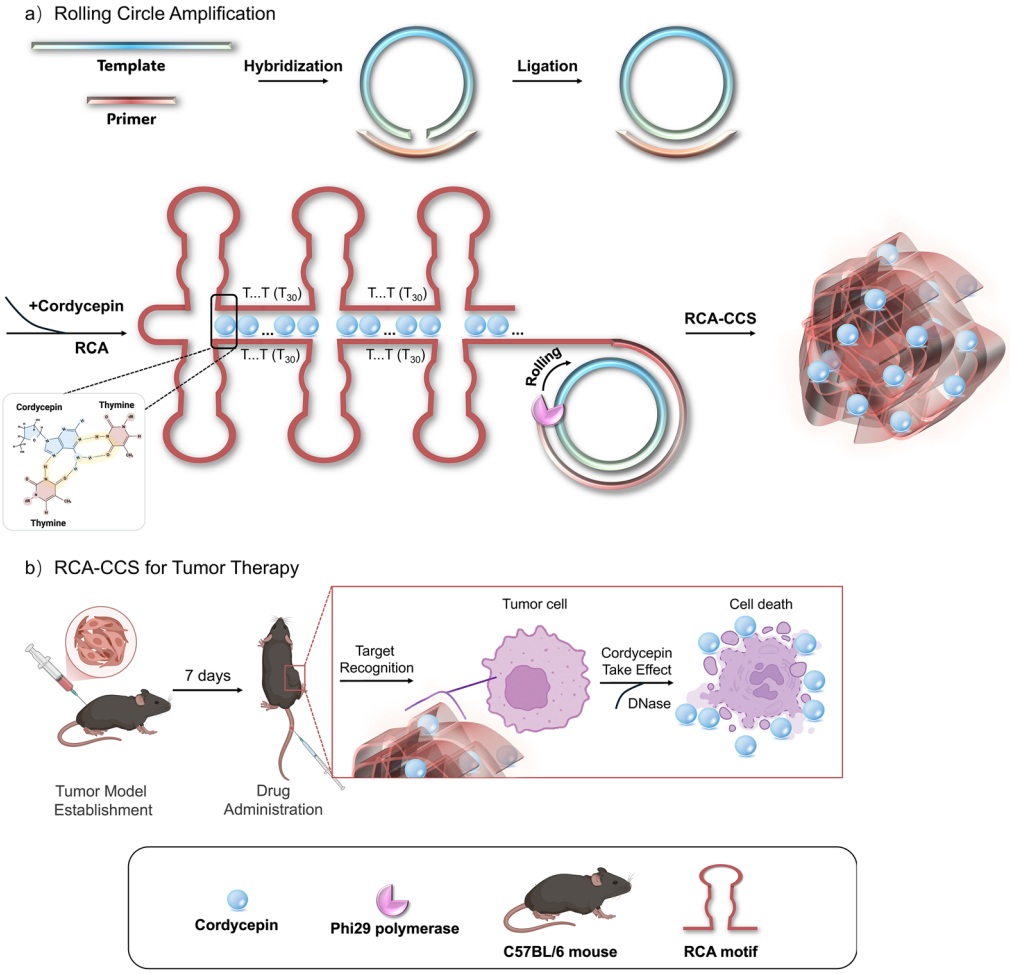

Fig. 2 Schematic illustration of the synthesis and anti-melanoma activity of RCA-CCS. (a) The template strand contained the complementary sequence of the MDR1-specific aptamer d_3 and A_{30} region. Through hybridization with the primer strand and ligation catalyzed *via* T_4 ligase, the template strand was circulated. The RCA process generated the elongated ssDNA, and cordycepin molecules were integrated through the formation of T–cordycepin–T triplets. (b) Following tumor model establishment, the administration of RCA-CCS inhibits tumor growth through the synergistic effect of aptamer d_3 and cordycepin.

biocompatibility of the RCA product (Fig. S10). In order to confirm the tumor cell specific-targeting and cellular uptake of RCA-CCS, human skin epithelial cell line HaCat was used as a control. Confocal imaging showed that the uptake of RCA-CCS was significantly higher in B16F10 cells compared to HaCat cells (Fig. 4a), which can be attributed to the overexpression of MDR1 on B16F10 cells. Subsequently, to evaluate the anti-tumor effects of RCA-CCS, B16F10 cells were exposed to varying concentrations of RCA-CCS and then stained with fixable viability dye. Flow cytometry results demonstrated a substantial growth inhibition when B16F10 cells were treated with RCA-CCS (Fig. 4b and c).

The *in vivo* anti-tumor efficacy of RCA-CCS was further evaluated in B16 melanoma-bearing mice. Following tumor establishment, the mice were randomly divided into six groups (n = 8 per group): a Model group (M) receiving PBS *via* intravenous injection; an Aptamer-only RCA Product group (RCA-Apt) administered intravenously; a Cordycepin group receiving 5 mg kg^{-1} *via* intragastric administration (CCS-i.g.); a Cordycepin group administered 5 mg kg^{-1} intravenously (CCS-i.v.); and two RCA-CCS groups receiving 0.05 mg kg^{-1} (RCA-CCS-low) or 0.1 mg kg^{-1} (RCA-CCS-high) cordycepin equivalents *via* intravenous injection, respectively. The treatments were conducted on day 7, 9, 11 and 13 (Fig. 5a).

Longitudinal monitoring of tumor volume (Fig. 5b) and photographs of tumor-bearing mice (Fig. S11) revealed significant growth suppression across treatment groups compared to the Model control. Notably, the RCA-CCS groups exhibited superior antitumor efficacy compared to both free cordycepin formulations. Critically, the intravenous administration of free cordycepin (CCS-i.v.) resulted in significantly reduced efficacy relative to the RCA-CCS groups, demonstrating that the enhanced therapeutic outcome is attributable to the nano-formulation rather than merely the route of administration. Furthermore, the RCA-Apt group showed no significant therapeutic effect, confirming that the observed antitumor activity is mediated specifically by the cordycepin payload rather than the aptamer or nucleic acid scaffold itself. The pronounced

 This journal is © The Royal Society of Chemistry 2026

Published on 28 Oktober 2025. Downloaded on 24.02.26 18:29:01.

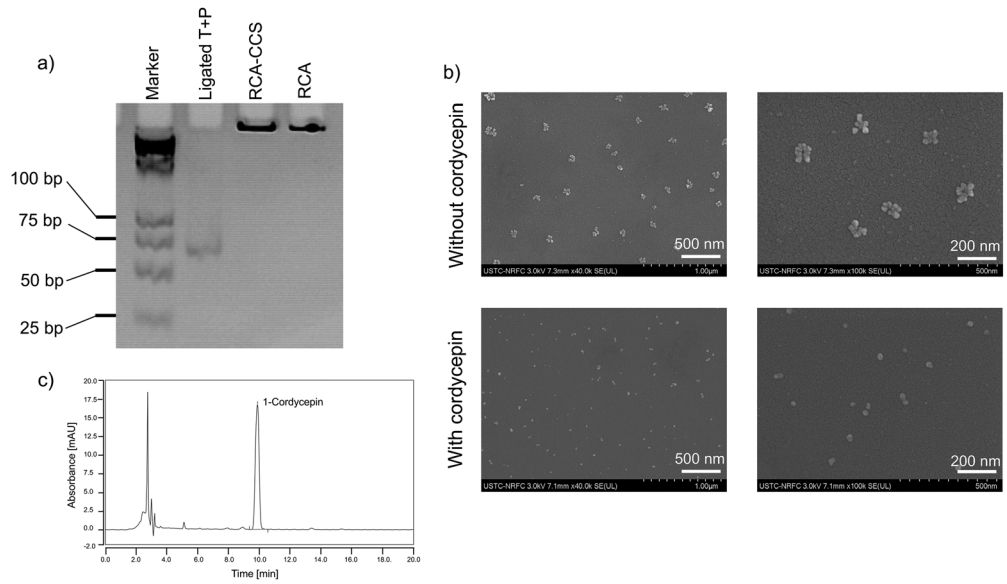

Fig. 3 (a) Native PAGE image indicating the formation of RCA-generated nanoparticles. Sample compositions and the band identities are indicated above and beside the gel images, respectively; (b) scanning electron microscopy images of RCA nanoparticles with (RCA-CCS) or without cordycepin; (c) chromatogram of the treated RCA-CCS solution. The amount of cordycepin in the sample was calculated from its peak area.

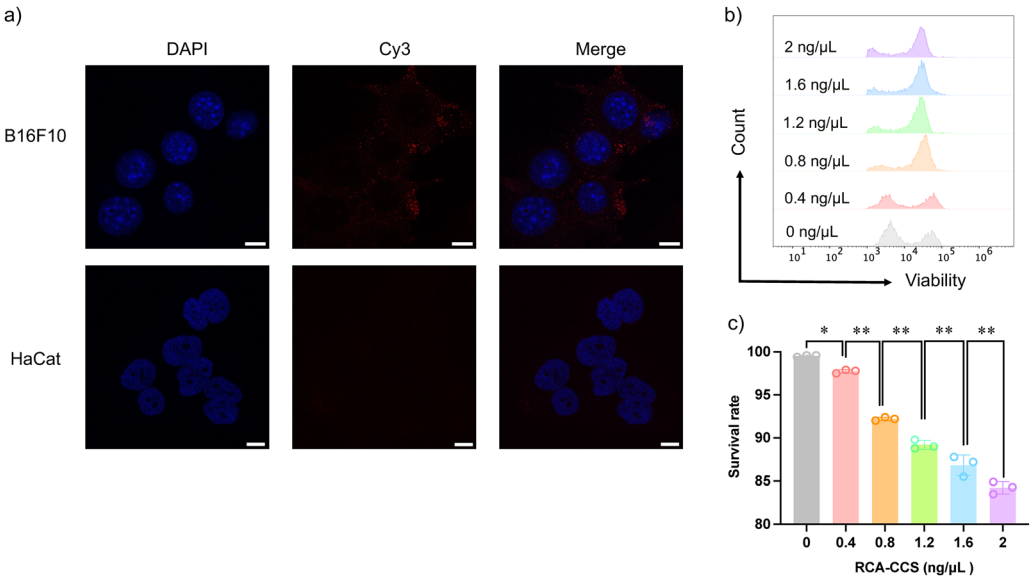

Fig. 4 (a) Confocal fluorescence images of B16F10 cells and HaCat cells treated with Cy3-labeled RCA-CCS for 2 hours. Scale bars are 10 μm. The red fluorescent signals from Cy3 labeling showed that the uptake of RCA-CCS was significantly higher in B16F10 cells compared to HaCat cells; (b) and (c) B16F10 cells were incubated with different concentrations of RCA-CCS for 24 hours. Cells were collected for apoptosis analysis by flow cytometry (b), and the survival rate (c) was calculated. Statistical analysis was performed using ordinary one-way ANOVA with multiple comparisons. Data are presented as mean ± s.d. (n = 3). *, $P < 0.05$; **, $P < 0.01$.

therapeutic efficacy of RCA-CCS can be attributed to two primary factors: (i) there is synergistic effect of cordycepin and the nucleic acid aptamer d_3, specifically targeting MDR1. The d_3 aptamer not only facilitated the delivery of cordycepin to tumors, but also blocked the multidrug resistance (MDR) of tumor cells, thereby increasing the accumulation of intracellular anticancer drugs. (ii) The RCA-generated nanocarrier significantly enhanced the efficiency of cordycepin cellular uptake.

On day 14, all the treated mice were sacrificed. The tumors were extracted and photographed (Fig. 5c). The mice in Model group which injected PBS exhibited a significant increase in both tumor size and weight. In contrast, the groups treated with RCA-CCS displayed a marked reduction in tumor size and weight (Fig. 5c and d). Analysis of tumor weight revealed inhibition rates of 63.9% and 76.2% in the RCA-CCS-low and RCA-CCS-high groups, respectively, when compared to the

Published on 28 Oktober 2025. Downloaded on 24.02.26 18:29:01.

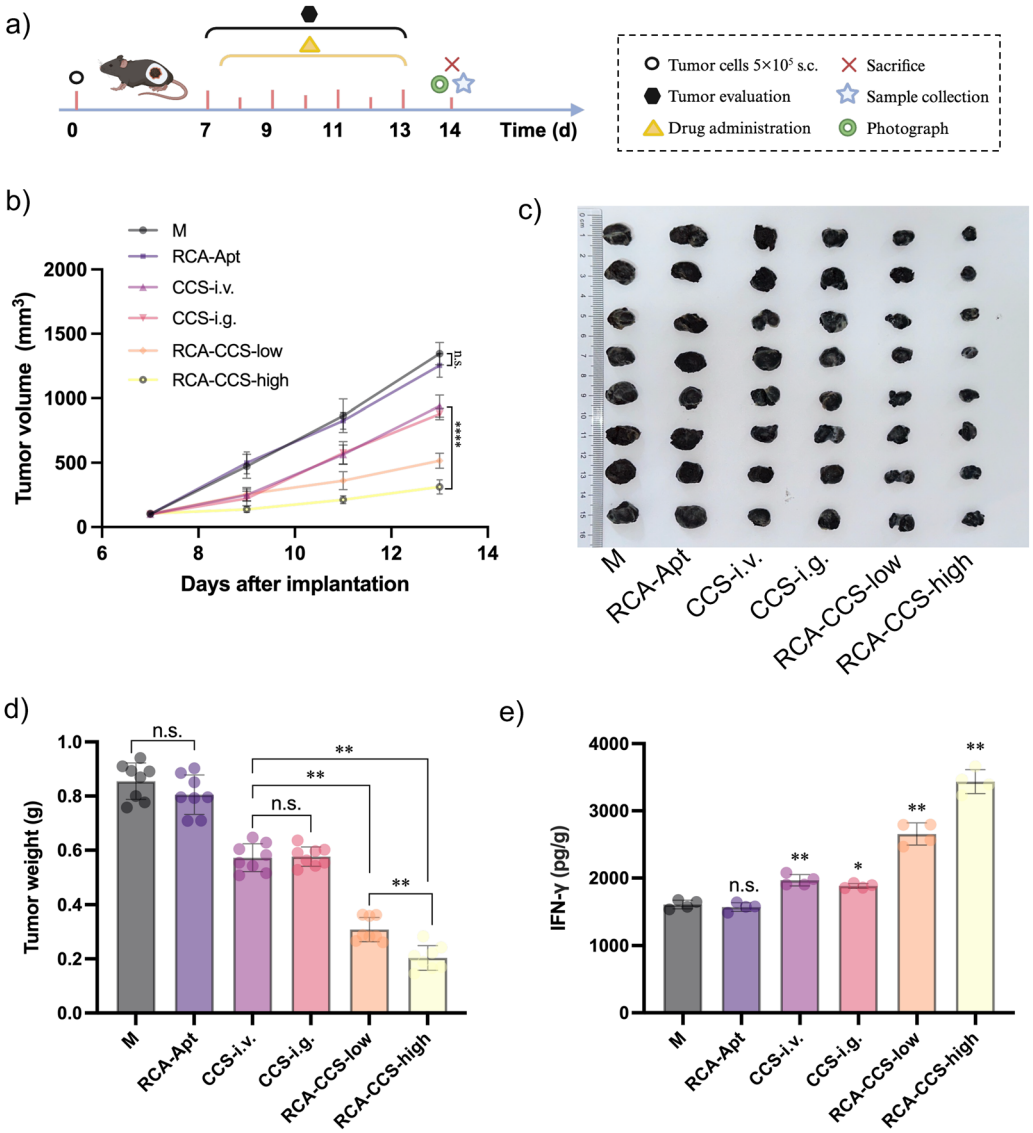

Fig. 5 Therapeutic effectiveness of RCA-CCS in an *in vivo* murine model of melanoma. (a) Schematic of tumor inoculation, treatment schedule, and time points for analysis of tumor growth; (b) changes in tumor volumes in different groups throughout the treatment period; (c) photograph of tumors dissected from mice in different groups; (d) statistical analysis of tumor weight in different groups; (e) ELISA was employed to examine the levels of IFN-γ. Data are presented as the mean ± s.d. (n = 8 in Fig. b and d and n = 4 in Fig. e) and statistical significance was determined using one-way analysis of variance (ANOVA). n.s., $P > 0.05$; *, $P < 0.05$; **, $P < 0.01$; ****, $P < 0.0001$.

Model group. Additionally, we measured the levels of interferon-γ (IFN-γ) in the tumor tissue as this cytokine plays pivotal roles in tumor progression. Enzyme-linked immunosorbent assays (ELISA) revealed that RCA-CCS notably elevated the secretion of IFN-γ (Fig. 5e), suggesting that RCA-CCS effectively bolstered the immune response and presented the anti-tumor effect. This immunomodulatory effect was complemented by significantly increased apoptosis in the RCA-CCS-high group, as evidenced by TUNEL staining (Fig. S12). To further assess systemic toxicity, the major organs (heart, liver, spleen, lung, and kidney) were harvested for histological analysis. H&E staining images showed no noticeable pathological changes in the major organs (Fig. S13).

3. Conclusion

In summary, we have developed a new strategy for the non-covalent integration of small molecule drugs into nucleic acid nanocarriers. To demonstrate its potential application, we constructed an RCA-based nanoparticle for the delivery of cordycepin and quantified its integration. By combining a MDR1-specific aptamer with cordycepin, the nanoparticle realized an efficient synergistic therapy for melanoma. Notably, many nucleosides and base analogues have the potential to mediate stable non-canonical DNA base-pairing. Our previous computational studies have identified several candidates, including fludarabine and sinefungin, that are promising for forming such triplet structures with a poly-T scaffold.[21]

This journal is © The Royal Society of Chemistry 2026

Published on 28 Oktober 2025. Downloaded on 24.02.26 18:29:01.

Concurrently, nucleoside and base analogues are an important category of anticancer and antiviral drugs due to their ability to disrupt the *in vivo* replication process of DNA. Therefore, by adopting this strategy, many other small molecule drugs beyond cordycepin can also be noncovalently incorporated into nucleic acid nanocarriers with precise content. This work presents a promising and generalizable method for the fabrication of synergistic nanodrugs that combine small molecule drugs with nucleic acid drugs.

4. Experimental section

4.1 Chemicals and materials

All oligonucleotides used in this work were purchased from Sangon Biotechnology Co., Ltd (Shanghai, China) and used without further purification. Their concentrations were quantified by UV absorbance at 260 nm. dNTP mixture (25 mM), phi29 DNA polymerase (10 U μL^{-1}), T4 DNA ligase (1000 U μL^{-1}), DAPI staining solution, antifade mounting medium, penicillin–streptomycin solution (penicillin 10 000 U mL^{-1}, streptomycin 10 mg mL^{-1}) and Deoxyribonuclease I (DNase I, 1 U μL^{-1}) were purchased from Beyotime Biotechnology (Shanghai, China). Fetal bovine serum (FBS), Dulbecco's modified Eagle's medium (DMEM), high glucose medium and RPMI-1640 medium were purchased from Wisent Inc. (Nanjing, China). Cordycepin and Cell Counting Kit-8 (CCK-8) were purchased from Topscience Co. Ltd (Shanghai, China). Cy3-dUTPs was purchased from ApexBio Technology. (USA). Fixable Viability Dye eFluor™ 520 was purchased from Thermo Fisher Scientific Inc. (Shanghai, China). ELISA Kits were purchased from Thermo Fisher Scientific Inc. (Shanghai, China).

4.2 TAE/Mg^{2+} buffer

1 × TAE/Mg^{2+} buffer (pH 8.0) consists of 40 mM tris base, 20 mM acetic acid, 2 mM EDTA, and 12.5 mM magnesium acetate. This buffer was used in the native PAGE and RCA-CCS sample wash.

4.3 Melting curve analysis

Melting measurement was carried out using a UV-vis spectrophotometer (Agilent, Cary 300, USA). T_{30} strands (2 μM) and cordycepin (300 μM) were dissolved in TAE/Mg^{2+} buffer and annealed from 50 °C to 4 °C over 2 h in advance. TAE/Mg^{2+} buffer with 300 μM cordycepin was used as a blank. The temperature was increased at a rate of 1 °C min^{-1} from 25 to 60 °C. The scatter plot of absorbance *versus* temperature was smoothed.

4.4 Synthesis of circular DNA template

The linear DNA template (0.6 μM) and DNA primer (0.6 μM) were mixed in 1 × ligation buffer. The total volume of the reaction was 50 μL. The mixture was slowly cooled from 95 °C to 22 °C over 2 hours using the polymerase chain reaction (PCR) machine for the hybridization of the template and the primer. The product was then incubated at 25 °C for 3 hours with T4 DNA ligase (10 U μL^{-1}) followed by incubation at 65 °C for 10 minutes to deactivate the enzyme.

4.5 Synthesis of RCA-CCS

The rolling circular amplification (RCA) system contained circular DNA template (0.3 μM), phi29 reaction buffer, phi29 DNA polymerase (2 U μL^{-1}), dNTPs (0.5 mM), and cordycepin (16 mM). The total volume of the reaction was 100 μL. The RCA reaction was carried out for 30 minutes at 30 °C to generate RCA products. The reaction mixture was then maintained at 75 °C for 10 minutes to inactivate the phi29 polymerase. For the synthesis of Cy3-labeled RCA-CCS, 10 μM Cy3-dUTPs was added into the reaction solution.

4.6 Morphology characterization of nanoparticles

The samples (30 μL) were gradient eluted using ethanol at varying concentrations (50%, 75%, 87.5%, 95%, 100%) for 3 minutes. Following each elution, the solution was centrifuged at 12 000 rpm for 12 minutes. After the final centrifugation, 30 μL of the supernatant was retained as the final product. The sample was then vortexed and evenly spread onto silicon. Subsequently, the samples were dried in a 37 °C oven for 12 hours and coated with Pt. A scanning electron microscope (Hitachi SU8220) was used to observe the sample.

4.7 Detection of cordycepin loading

The RCA-CCS sample was extensively washed by ultrafiltration using 1 mL MerckMillipore ultrafiltration tubes (UFC5010BK, MW cut-off 10 kDa) to remove excess cordycepin. 1 × TAE/Mg^{2+} buffer was used as washing buffer. DNase I was then added to the sample followed by incubation at 37 °C for 12 hours to cleave the RCA structure and release cordycepin. The sample was then heated at 65 °C for 10 minutes with 25 mM EDTA to deactivate DNase I. Finally, 5 mL double-distilled water was added to dilute the products. Nanodrop was used to determine the concentration of DNA. The amount of cordycepin in the sample was analyzed by high-performance liquid chromatography (HPLC) (Thermofisher Scientific, Ultimate 3000). The analysis conditions of HPLC were as follows: injection volume: 10 μL; mobile phase A: acetonitrile; mobile phase B: H_2O; mobile phase ratio: mobile phase A : mobile phase B = 5 : 95; chromatographic column: Thermo Syncronis C18 (250 × 4.6 mm, 5 μm). The loading ratio of cordycepin in RCA-CCS was calculated according to the amount of DNA and cordycepin in the sample (Fig. S8).

4.8 Native PAGE

Native PAGE that contained 15% or 8% polyacrylamide (19 : 1 acrylamide : bisacrylamide) was run on a DYY-6C electrophoresis unit (Beijing Liuyi Biotechnology Co., Ltd) at 20 °C (100 V, constant voltage). 1 × TAE/Mg^{2+} buffer was used as a running buffer. After electrophoresis, the gels were stained with Stains-All (BBI Life Science) or Gelred (BBI Life Science) and imaged with a gel image system (Tanon 1600).

15% native PAGE was used for the verification of the formation of cordycepin mediated T–T base pairing.

8% native PAGE was used for the characterization of the hybridization of RCA template and primer.

Published on 28 Oktober 2025. Downloaded on 24.02.26 18:29:01.

4.9 Serum stability test of RCA products

RCA products were washed by ultrafiltration using 1 mL MerckMillipore ultrafiltration tubes to remove excess reactant. Subsequently, 20 μL washed products were added into 200 μL 10% FBS. The mixtures were incubated at 37 °C for 12 hours, 24 hours, and 48 hours, respectively. At the end of the incubations, samples were centrifuged and analyzed by 8% native PAGE (100 V voltage, constant voltage).

4.10 Cell culture

B16F10 cells were purchased from Procell Life Science & Technology Co., Ltd (Wuhan, China). B16F10 cells were cultured in RPMI-1640 medium added with 10% FBS and 1% penicillin–streptomycin solution at 37 °C in a humid atmosphere with 5% CO_2. HaCat cells were purchased from FuHeng BioLogy (Shanghai, China). HaCat cells were cultured in DMEM with added 10% FBS and 1% penicillin–streptomycin solution at 37 °C in a humid atmosphere with 5% CO_2.

4.11 Cell viability

The effect of the materials on cell viability of B16F10 cells was tested using CCK-8. B16F10 cells were plated in 96-well plates with 1×10^5 cells per well. 0.8 ng μL^{-1}, 1.6 ng μL^{-1}, 2.4 ng μL^{-1}, 3.2 ng μL^{-1}, and 4 ng μL^{-1} RCA products were added to wells, respectively. After 24 hours' incubation, the supernatant in the wells was discarded. 10 μL of CCK-8 solution and 90 μL of culture medium were then added to each well and incubated for 2 hours at 37 °C. The absorbance of the samples was measured at 450 nm using microplate reader (Super Max3100). Cell viability was expressed as a percentage value of the absorbance values of the experimental and control groups. All experiments were carried out with five replicates.

4.12 Flow cytometric analysis

Flow cytometric analysis was applied to quantify the cell viability of B16F10 cells after treatment with RCA-CCS for 24 hours. Untreated cells were used as the negative control. Cells were then suspended in PBS and stained with Fixable Viability Dye according to the protocol supplied by the manufacturer (Invitrogen). The fluorescence signal of the cells was analyzed using flow cytometry (BD, FACSCanto).

4.13 Characterization of specific cell-targeting

The specific targeting of B16F10 cells was verified by fluorescence microscopy imaging of cells incubated with Cy3-labeled nanocarriers. HaCat cells were used as a negative control. The cell climbing slices were pre-treated in 75% alcohol for 5 minutes, following flame-drying over an alcohol lamp. The cell climbing slices were placed in a 24 well-plate before cell seeding. Both of the cells were seeded at 1×10^6 cells per well. After 24 hours culturing, 30 nM Cy3-labeled RCA-CCS was added into each well. After 2 hours of incubation, the cells were washed with PBS and fixed with 4% paraformaldehyde (PFA) at 4 °C for 30 minutes. Subsequently, the liquid was removed, and the nuclei were stained with DAPI staining solution at 4 °C for 5 minutes. Finally, the cell climbing slides were taken out from the plate and fixed on a glass slide for observation by laser confocal microscopy (Leica, sp8).

4.14 Animal experiment

Six-week-old female C57BL/6 mice were purchased from Gem-Pharmatech LLC. Mice were housed under specific pathogen-free conditions at 22–24 °C and given unlimited access to food and water. Experiments were conducted after one week of adaptive rearing. All animal experiments were performed in strict accordance with the Guide for the Care and Use of Laboratory Animals and have received approval from Animal Investigation Ethics Committee of Anhui Medical University (approval number: PZ-2024-046). A suspension containing 5×10^5 B16F10 mouse melanoma cells in PBS was subcutaneously injected into the back region of each mouse, and the subcutaneous tumor model was established when the tumor volume reached 100 mm^3. The mice were then randomly divided into six groups (n = 8): a Model group (M) receiving PBS *via* intravenous injection; an Aptamer-only RCA Product group (RCA-Apt) administered intravenously; a Cordycepin group receiving 5 mg kg^{-1} *via* intragastric administration (CCS-i.g.); a Cordycepin group administered 5 mg kg^{-1} intravenously (CCS-i.v.); and two RCA-CCS groups receiving 0.05 mg kg^{-1} (RCA-CCS-low) or 0.1 mg kg^{-1} (RCA-CCS-high) cordycepin equivalents *via* intravenous injection, respectively. These treatments were administered on day 7, 9, 11 and 13.

During the experiment, tumor volume, body weight, clinical signs, and food intake were regularly monitored. The tumor size was quantified with the formula $V = a \times b^2/2$, where a and b were the tumor length and width. When the tumor size in Group M reached a volume of approximately 1500 mm^3, the experiments were discontinued and mice were sacrificed. The tumors were removed, weighed, and photographed. The major organs (heart, liver, spleen, lung, kidney) were removed, and stored in 4% paraformaldehyde.

4.15 ELISA assays

To examine the intratumor levels of interferon-gamma (IFN-γ), single cell suspensions of B16F10 transplanted tumors were obtained by rapid and gentle stripping, physical grinding in cold PBS and filter filtration. IFN-γ was detected with an ELISA kit according to the manufacturer's guidelines.

4.16 Statistical analysis

Data were analyzed statistically and presented as mean ± standard deviation. The one-way ANOVA with multiple comparisons was employed for group comparisons using Prism 8.0 software (GraphPad). A p-value below 0.05 denotes statistical significance.

Ethics statement

All animal experiments were performed in strict accordance with the Guide for the Care and Use of Laboratory Animals

 This journal is © The Royal Society of Chemistry 2026

Published on 28 Oktober 2025. Downloaded on 24.02.26 18:29:01.

and have received approval from Animal Investigation Ethics Committee of Anhui Medical University (approval number: PZ-2024-046).

Author contributions

All authors have contributed significantly to this work and approved the final version of the manuscript. The specific contributions are as follows: conceptualization: Z. J. M., W. S.; methodology: F. X. Y., Z. M. T., J. L. Y., S. R., W. Y. Y.; visualization: L. W. T., C. H. C., L. M. M., W. S. H., M. Y. X.; supervision: Z. J. M., W. S., C. X., S. W. Y.; writing – original draft: Z. J. M.; writing – review & editing: Z. J. M., W. S., C. X., S. W. Y.

Conflicts of interest

The authors declare no conflict of interests.

Data availability

All data generated or analyzed during this study are included in the article and its supplementary information (SI). Supplementary information: additional tables and additional figures. See DOI: **https://doi.org/10.1039/d5nh00489f**.

Acknowledgements

Financial support was provided by the National Natural Science Foundation of China (52303168), the Natural Science Foundation of Anhui Province (2308085QE145), the Natural Science Research Project of Anhui Educational Committee (2024AH030025), the Postgraduate Innovation Research and Practice Program of Anhui Medical University (YJS20240039), the Fundamental Research Funds for the Central Universities (WK2060000094), Research Level Improvement Program of Anhui Medical University (2021xkjT016), Natural Science Research of Higher Education Institutions of Anhui Province (2024AH050797), Anhui Clinical and Translational Medicine Research Project (202204295107020030), and Anhui Province Excellent Research and Innovation Team Project (2024AH 010013). This work was partially carried out at the USTC Center for Micro and Nanoscale Research and Fabrication.

References

1 C. He, K. Lu, D. Liu and W. Lin, Nanoscale metal–organic frameworks for the co-delivery of cisplatin and pooled siRNAs to enhance therapeutic efficacy in drug-resistant ovarian cancer cells, *J. Am. Chem. Soc.*, 2014, **136**, 5181–5184.

2 Y. Chen, Y. Huang, Q. Li, Z. Luo, Z. Zhang, H. Huang, J. Sun, L. Zhang, R. Sun, D. J. Bain, J. F. Conway, B. Lu and S. Li, Targeting Xkr8 via nanoparticle-mediated in situ co-delivery of siRNA and chemotherapy drugs for cancer immunochemotherapy, *Nat. Nanotechnol.*, 2023, **18**, 193–204.

3 K. Butowska, X. Han, N. Gong, R. El-Mayta, R. M. Haley, L. Xue, W. Zhong, W. Guo, K. Wang and M. J. Mitchell, Doxorubicin-conjugated siRNA lipid nanoparticles for combination cancer therapy, *Acta. Pharm. Sin. B*, 2023, **13**, 1429–1437.

4 A. S. Desai, D. J. Webb, J. Taubel, S. Casey, Y. Cheng, G. J. Robbie, D. Foster, S. A. Huang, S. Rhyee, M. T. Sweetser and G. L. Bakris, Zilebesiran, an RNA interference therapeutic agent for hypertension, *N. Engl. J. Med.*, 2023, **389**, 228–238.

5 G. L. Bakris, M. Saxena, A. Gupta, F. Chalhoub, J. Lee, D. Stiglitz, N. Makarova, N. Goyal, W. Guo, D. Zappe and A. S. Desai, KARDIA-1 Study Group, RNA interference with zilebesiran for mild to moderate hypertension: The KARDIA-1 randomized clinical trial, *JAMA*, 2024, **331**, 740–749.

6 Q. D. Nguyen, R. A. Schachar, C. I. Nduaka, M. Sperling, K. J. Klamerus, K. Chi-Burris, E. Yan, D. A. Paggiarino, I. Rosenblatt, R. Aitchison, S. S. Erlich and MONET Clinical Study Group, Evaluation of the siRNA PF-04523655 versus ranibizumab for the treatment of neovascular age-related macular degeneration (MONET Study), *Ophthalmology*, 2012, **119**, 1867–1873.

7 Q. Hu, H. Li, L. Wang, H. Gu and C. Fan, DNA nanotechnology-enabled drug delivery systems, *Chem. Rev.*, 2019, **119**, 6459–6506.

8 L. Lin, P. Wei, T. Kong, B. Yuan, P. Fu, Y. Li, Y. Wang, J. Zheng and K. Wang, Framework nucleic acid-programmed aptamer-paclitaxel conjugates as targeted therapeutics for triple-negative breast cancer, *Nanoscale Horiz.*, 2025, **10**, 873–884.

9 Q. Tang, Q. Li, L. Shi, W. Liu, B. Li and Y. Jin, Multifunctional DNA nanoprobe for tumor-targeted synergistic therapy by integrating chemodynamic therapy with gene silencing, *Nanoscale Horiz.*, 2023, **8**, 1106–1112.

10 S. Xie, W. Sun, T. Fu, X. Liu, P. Chen, L. Qiu, F. Qu and W. Tan, Aptamer-based targeted delivery of functional nucleic acids, *J. Am. Chem. Soc.*, 2023, **145**, 7677–7691.

11 M. Hu, C. Feng, Q. Yuan, C. Liu, B. Ge, F. Sun and X. Zhu, Lantern-shaped flexible RNA origami for Smad4 mRNA delivery and growth suppression of colorectal cancer, *Nat. Commun.*, 2023, **14**, 1307.

12 X. Ma, J. Yan, G. Zhou, Y. Li, M. Ran, C. Li, X. Chen, W. Sun, H. Zhang and X. Shen, Fabrication of metal nuclear acid framework to enable carrier-free MNAzyme self-delivery for gastric cancer treatment, *Adv. Funct. Mater.*, 2024, **34**, 2406650.

13 H. Zhang, L. Zhang, Z. Cao, S. Cheong, C. Boyer, Z. Wang, S. L. J. Yun, R. Amal and Z. Gu, Two-dimensional ultra-thin nanosheets with extraordinarily high drug loading and long blood circulation for cancer therapy, *Small*, 2022, **18**, 2200299.

14 Y. Yang, B. Sun, S. Zuo, X. Li, S. Zhou, L. Li, C. Luo, H. Liu, M. Cheng, Y. Wang, S. Wang, Z. He and J. Sun, Trisulfide bond-mediated doxorubicin dimeric prodrug nanoassemblies with high drug loading, high self-assembly stability, and high tumor selectivity, *Sci. Adv.*, 2020, **6**, eabc1725.

Published on 28 Oktober 2025. Downloaded on 24.02.26 18:29:01.

15 W. Yang, Q. Sun, X. Zhang, L. Zheng, X. Yang, N. He, Y. Pang, X. Wang, Z. Lai, W. Zheng, S. Zheng and W. Wang, A novel doxorubicin/CTLA-4 blocker co-loaded drug delivery system improves efficacy and safety in antitumor therapy, *Cell Death Dis.*, 2024, **15**, 386.
16 Z. Zhao, Y. Dong, Z. Duan, D. Jin, W. Yuan and D. Liu, DNA-organic molecular amphiphiles: Synthesis, self-assembly, and hierarchical aggregates, *Aggregate*, 2021, **2**, e95.
17 J. Zhang, Y. Guo, F. Ding, G. Pan, X. Zhu and C. Zhang, A camptothecin-grafted DNA tetrahedron as a precise nanomedicine to inhibit tumor growth, *Angew. Chem., Int. Ed.*, 2019, **58**, 13794–13798.
18 L. Zhu, Y. Guo, Q. Qian, D. Yan, Y. Li, X. Zhu and C. Zhang, Carrier-free delivery of precise drug-chemogene conjugates for synergistic treatment of drug-resistant cancer, *Angew. Chem., Int. Ed.*, 2020, **59**, 17944–17950.
19 Q. Mou, Y. Ma, F. Ding, X. Gao, D. Yan, X. Zhu and C. Zhang, Two-in-one chemogene assembled from drug-integrated antisense oligonucleotides to reverse chemoresistance, *J. Am. Chem. Soc.*, 2019, **141**, 6955–6966.
20 Q. Li, J. Zhao, L. Liu, S. Jonchhe, F. J. Rizzuto, S. Mandal, H. He, S. Wei, H. F. Sleiman, H. Mao and C. Mao, A poly-(thymine)-melamine duplex for the assembly of DNA nanomaterials, *Nat. Mater.*, 2020, **19**, 1012–1018.
21 X. Feng, X. Wang, J. Liu, A. Fu, Y. Wang, S. Wei, H. Chen, R. She, Y. Wang, X. Cui, H. Hou, Y. Xu, Y. Wu, Q. Meng, L. Zhang, S. Wang and J. Zhao, Accelerated screening of alternative DNA base-organic molecule-base architectures via integrated theory and experiment, *Angew. Chem., Int. Ed.*, 2024, **63**, e202408003.
22 C. Lachance-Brais, M. Rammal, J. Asohan, A. Katolik, X. Luo, D. Saliba, A. Jonderian, M. J. Damha, M. J. Harrington and H. F. Sleiman, Small molecule-templated DNA hydrogel with record stiffness integrates and releases DNA nanostructures and gene silencing nucleic acids, *Adv. Sci.*, 2023, **10**, 2205713.
23 L. Chang, R. Zhang, J. Wang, C. Yao and D. Yang, Construction of polymeric DNA network and application for cell manipulation, *Chin. J. Chem.*, 2023, **41**, 1875–1887.
24 Z. Lv, Z. Li, P. Li, C. Yao and D. Yang, DNA nanomaterials for delivery of clustered regularly interspaced short palindromic repeats/Cas systems, *Small Struct.*, 2023, **4**, 2300086.
25 R. Hu, X. Zhang, Z. Zhao, G. Zhu, T. Chen, T. Fu and W. Tan, DNA nanoflowers for multiplexed cellular imaging and traceable targeted drug delivery, *Angew. Chem., Int. Ed.*, 2014, **53**, 5821–5826.
26 F. Li, N. Song, Y. Dong, S. Li, L. Li, Y. Liu, Z. Li and D. Yang, A proton-activatable DNA-based nanosystem enables co-delivery of CRISPR/Cas9 and DNAzyme for combined gene therapy, *Angew. Chem., Int. Ed.*, 2022, **61**, e202116569.
27 C. Yao, R. Zhang, J. Tang and D. Yang, Rolling circle amplification (RCA)-based DNA hydrogel, *Nat. Protoc.*, 2021, **16**, 5460–5483.
28 Y. Huang, X. Liu, J. Zhu, Z. Chen, L. Yu, X. Huang, C. Dong, J. Li, H. Zhou, Y. Yang and W. Tan, Enzyme core spherical nucleic acid that enables enhanced cuproptosis and anti-tumor immune response through alleviating tumor hypoxia, *J. Am. Chem. Soc.*, 2024, **146**, 13805–13816.
29 X. Wen, Z. Huang, X. Yang, X. He, L. Li, H. Chen, K. Wang, Q. Guo and J. Liu, Development of an aptamer capable of multidrug resistance reversal for tumor combination chemotherapy, *Proc. Natl. Acad. Sci. U. S. A.*, 2024, **121**, e2321116121.
30 K. M. Hanssen, M. Haber and J. I. Fletcher, Targeting multidrug resistance-associated protein 1 (MRP1)-expressing cancers: beyond pharmacological inhibition, *Drug Resist. Updat.*, 2021, **59**, 100795.
31 Q. Tang, S. Leng, Y. Tan, H. Cheng, Q. Liu, Z. Wang, Y. Xu, L. Zhu and C. Wang, Chitosan/dextran-based organohydrogel delivers EZH2 inhibitor to epigenetically reprogram chemo/immuno-resistance in unresectable metastatic melanoma, *Carbohydr. Polym.*, 2024, **346**, 122645.

 This journal is © The Royal Society of Chemistry 2026